# A level set model for delamination – Modeling crack growth without cohesive zone or stress singularity

Frans van der Meer, Nicolas Moes, Lambertus J Sluys

# A level set model for delamination – Modeling crack growth without cohesive zone or stress singularity

F.P. van der Meer [a,b,*], N. Moës [b], L.J. Sluys [a]

[a] Delft University of Technology, Faculty of Civil Engineering and Geosciences, PO Box 5048, 2600 GA Delft, The Netherlands
[b] Ecole Centrale de Nantes, GeM Institute, UMR CNRS 6183, 1 Rue de la Noë, 44321 Nantes, France

A new method is presented for the modeling of progressive delamination which allows for the use of elements that are larger than the cohesive zone. The central idea is that the crack front location is described implicitly with a level set field and the cohesive zone reduces to a line. This means that the crack front does not have to be aligned with the element bound-aries. At the crack front, weak discontinuities are inserted in the displacement to allow for a sharp transition between the cracked and uncracked parts. The weak discontinuity is derived from a strong discontinuity formulation and the most favorable technique for gap closure is investigated. Crack growth is handled with an explicit energy-based relation, in which the configurational force is computed as the jump in Eshelby tensor over this transition. The same energy-based criterion is used to predict initiation along the free edge. In numerical examples results are compared with analytical solutions and results from computational cohesive zone analyses.

## 1. Introduction

Delamination is one of the main failure processes in composite laminates. It may appear as a consequence of out-of-plane impact, it may arise due to the stress transfer near transverse matrix cracks through the thickness of the plies, or it may grow from the free edge due to the mismatch in thermal and lateral contraction properties of neighboring plies with differing fiber orientation. As a consequence of delamination, the plies are no longer cooperating as they were designed to be, and the mechanical properties of the laminate deteriorate. This is the case for in-plane loading, but particularly strong for out-of-plane loading. Therefore, the simulation of delamination growth is of interest for composites design and engineering.

In current computational practice, delamination is most often modeled by means of interface elements, as first done by Allix and Ladevèze [1] and Schellekens and De Borst [2] and later by many others, see e.g. [3–8]. Central in this approach is the relation between the separation of the crack surfaces and the traction that is applied on the crack surfaces. This relation typically consists of an initial stiff and elastic part, followed by a softening part. During crack growth, there is a zone in which the material is in the softening regime. This is the so-called cohesive zone. The traction–separation relation can be related to the strength of the interface via the maximum traction, and to its fracture toughness via the area under the curve. As such, both initiation and propagation of delamination are dealt with in a rather simple single model.

However, this approach has one limiting requirement, which is that a fine in-plane discretization is required. For stability and accuracy, it is necessary that the cohesive zone is meshed with several elements. And since the cohesive zone moves

* Corresponding author at: Delft University of Technology, Faculty of Civil Engineering and Geosciences, PO Box 5048, 2600 GA Delft, The Netherlands. Tel.: +31 (0)15 278 5918; fax: +31 (0)15 278 5767.

*E-mail addresses:* f.p.vandermeer@tudelft.nl (F.P. van der Meer), n.moes@ec-nantes.fr (N. Moës), l.j.sluys@tudelft.nl (L.J. Sluys).

**Nomenclature**

*Latin characters*

| | |
|---|---|
| $a$ | crack length |
| $\mathbb{C}$ | material tangent tensor |
| $\mathbf{d}$ | nodal displacement vector |
| $E$, $E_1$, $E_2$ | Young's moduli |
| $\mathbf{f}$ | force vector |
| $F$ | total external load |
| $g$ | energy release per unit volume front movement |
| $G$ | energy release per unit area crack growth |
| $G_c$ | fracture toughness |
| $G_{12}$,$G_{13}$ | Shear moduli |
| $h$ | typical element size |
| $\mathbf{I}$ | identity tensor |
| $\mathbf{K}$ | global stiffness matrix |
| $l$ | specimen length |
| $\mathbf{l}$ | nodal Lagrange multiplier vector |
| $n$ | number of nodes |
| $\mathbf{n}$ | normal vector to crack front |
| $\mathbf{N}$ | shape function matrix (vector field) |
| $\overline{\mathbf{N}}$ | shape function vector (scalar field) |
| $\mathbf{M}$ | resistance matrix against crack growth |
| $\mathbf{P}$ | Eshelby tensor |
| $s$ | parametrized crack front coordinate |
| $\mathbf{s}$ | tangent vector to crack front |
| $t$ | specimen thickness |
| $\mathbf{t}$ | traction |
| $\mathbf{t}_N$ | prescribed external traction |
| $u$ | (prescribed) displacement value |
| $\dot{u}$ | applied displacement rate |
| $\mathbf{u}$ | displacement field |
| $v_n$ | normal velocity field |
| $\mathbf{v}_n$ | nodal normal velocity vector |
| $w$ | specimen width |
| $x$, $y$, $z$ | spatial coordinates with $x$ and $y$ in the plane of the laminate |
| $\mathbf{x}$ | spatial coordinate vector |

*Greek characters*

| | |
|---|---|
| $\beta$ | interaction coefficient for Nitsche's method |
| $\delta$ | variation operator |
| $\Delta t$ | time step size |
| $\Delta t^0$ | initial time step size |
| $\Delta u^0$ | initial displacement increment size |
| $\varepsilon$ | strain tensor |
| $\epsilon$ | error |
| $\Gamma$ | surface domain through the thickness of the laminate at front location |
| $\Gamma_N$ | boundary domain on which prescribed traction is applied |
| $\overline{\Gamma}$ | 2D projection of $\Gamma$ |
| $\theta$ | penalty parameter |
| $\kappa$ | stabilization parameter |
| $\lambda$ | lagrange multiplier field |
| $\mu$ | crack growth resistance parameter |
| $\nu_{12}$ | in-plane Poisson's ratio |
| $\Pi$ | potential energy |
| $\sigma$ | stress tensor |
| $\phi$ | level set field |
| $\psi$ | strain energy density |
| $\Omega$ | volume domain |
| $\overline{\Omega}$ | 2D projection of $\Omega$ |

*Other symbols and sub/superscripts*

| | |
|---|---|
| $\nabla$ | gradient operator |
| $\nabla_s$ | symmetric gradient operator |
| $[\![\bullet]\!]$ | jump operator |
| $\langle\bullet\rangle_\beta$ | weighting operator for Nitsche's method |
| $\langle\bullet\rangle_+$ | McCauley brackets (positivity constraint) |
| $\bullet^+$ | related to cracked subdomain |
| $\bullet^-$ | related to uncracked subdomain |
| $\bullet_{\text{top}}$ | related to top sublaminate |
| $\bullet_{\text{bot}}$ | related to bottom sublaminate |

*Abbreviations*

| | |
|---|---|
| 1D, 2D, 3D | one/two/three dimensional |
| VCCT | virtual crack closure technique |
| X-FEM | extended finite element method |

through the domain during delamination growth, the part of the domain where a fine mesh is necessary can be large, or remeshing has to be applied. Given that the cohesive zone length for delamination in composite laminates is typically of the order of 1 mm [5], this puts a severe restriction on the dimensions of the problems that can be analyzed numerically against acceptable computation costs.

This cannot easily be resolved by modeling the crack with the eXtended Finite Element Method (X-FEM), a method that allows discontinuities to run through the finite elements. Most commonly this method is combined with asymptotic enrichment functions to accurately represent the singular stress field near the crack tip [9], which has been applied in the context of delamination by Esna Ashari and Mohammadi [10]. For laminates however, representation of the singular stress field requires an even finer discretization around the crack tip than the cohesive approach, particularly through the thickness of the laminate. Alternatively X-FEM can be combined with cohesive tractions, as has been done in the context of delamination by Wells et al. [11] and Remmers et al. [12], but this approach suffers from the same requirement on the in-plane element size as the use of interface elements.

In the context of interface elements, several strategies have been proposed to allow for the use of larger elements in delamination problems. One crude solution is to add viscosity to the traction–separation law as done by Chaboche et al. [13]. In this way the fracture toughness is artificially increased, with uncertain influence on the global behavior. Alternatively, Turon et al. [14] have proposed to artificially increase the cohesive zone length by reducing the interface strength parameter while keeping the fracture toughness constant. This technique is certainly meritable for its simplicity, but a later study by Harper and Hallett [15] has shown that its applicability without loss of accuracy is limited even in simple cases, and Van der Meer et al. [16] have reported a significant influence of the moderate changes in the interface strength on the peak load in more complex cases.

Instead of changing model parameters, Yang et al. [17] have proposed to use a richer integration scheme close to the crack front. This does improve the stability of the response to some extent, but the core issue, that the discretization of the displacement field around the front is too coarse to describe the solution, is not addressed.

Another direction to improve the performance of large interface elements is to locally enrich the displacement field. Improvement was already reported by Crisfield and Alfano [18] with a relatively simple hierarchical enrichment. Guiamatsia et al. [19] enriched the displacement field with the analytical solution of a beam on elastic foundation. This was based on the assumption that it is underrepresentation of the variation of the stress ahead of the crack tip which needs to be addressed. However, the real challenge is to enrich the kinematics such that deformation of an element containing the crack tip can be represented accurately, resulting in a smooth response for a smooth progression of the crack tip through the element. Such an enrichment scheme has been proposed by Samimi et al. [20], who added a hat-enrichment where the location of the peak of the enrichment is another degree of freedom. However, this strategy has only been shown to work in 2D with line interfaces; generalization to cases with plane interfaces is not obvious.

In contrast with all mentioned strategies to solve the cohesive zone with relatively large elements, we choose in this work to start from a fracture mechanics point of view, where the crack front is a line instead of a band. Where adding viscosity or reducing the interface strength improves stability by increasing the length of the cohesive zone when the elements cannot be chosen smaller than that zone, we start from the other end, supposing that the cohesive zone length is smaller than the element size. In fact, in order to analyze large scale delamination, one is not interested in what is happening inside the cohesive zone, apart from the fact that a certain amount of energy is dissipated during crack growth. As remarked by Willis, "the Barrenblatt [cohesive] approach has no great advantage over that of Griffith [fracture mechanics], if used just to predict growth" [21]. Obviously, when trying to eliminate the cohesive zone from the analysis, one will have to turn to fracture mechanics to model crack growth.

There already exists one method in which the crack front is modeled as a line and an energy based criterion is used to predict crack growth, namely the virtual crack closure technique (VCCT). This method, introduced by Rybicki and Kanninen

[22], is based on Irwin's theory, that the amount of energy dissipated during crack growth over a small distance is equal to the energy required to close the crack over the same distance [23]. For an historic review of the VCCT we refer to Krueger [24]. Although initiation is fundamentally excluded, this technique is very efficient for the assessment of crack growth criteria on a predefined crack. However, for the modeling of progressive failure it has several drawbacks. Firstly, the node-to-node basis of crack growth leads to a non-smooth global response. Secondly, the fact that the crack front remains aligned with the mesh implies that a poor representation of the crack front will arise for crack growth that is not self-similar, leading to poor estimates of the energy release along the crack front. Nevertheless, several examples of successful progressive delamination analyses based on VCCT-models can be found in literature [25–27].

In the context of the VCCT, Zou et al. [28] have pointed out that when laminate theory is applied, i.e. when high order gradients are eliminated from the through thickness variations in displacement, the stress singularity around the crack tip is eliminated. The singularity is transformed into discontinuities in stress over the plane through the thickness of the laminate. In later publications, Zou et al. have shown that this jump in stress can be used as a configurational force that drives crack growth [29,30], although the VCCT requirement that the delamination front is located on the element edges was not overcome.

In this paper, a new approach to delamination modeling is presented, in which, in contrast with cohesive models, the crack front is represented as a line, and, in contrast with the VCCT, the crack front can be arbitrarily shaped and can grow continuously. For this purpose, the level set method is applied, a method with many applications in the mesh-independent representation of moving fronts [31]. In the level set method, a scalar field is defined, and the line where this field is equal to zero is taken to be the front. Thus, the front is implicitly described and does not have to match the element boundaries.

The model is comprised of two submodels that are solved in a staggered fashion. Firstly, there is the finite element model of a partially cracked medium. This submodel contains a special kinematic formulation for those elements that contain the crack front, which will be introduced in Section 2. Secondly, there is the crack growth model, which takes the displacement field from the first submodel and computes the front velocity via energy release relations. Next, the crack is updated and the new front location is given to the first submodel, and so on. The second submodel will be the subject matter of Section 3. Furthermore, the issue of initiation will be addressed in Section 4. In Section 5 the global algorithm will be summarized, after which the validity of the approach will be demonstrated with several numerical examples in Section 6.

For simplicity, the model is only presented in 2D, focusing on the plane of the laminate (the $(x,y)$-plane). In this, the issue of how to represent an arbitrarily located crack front in the interface plane is emphasized. This issue has not yet been addressed in previous enrichment strategies for delamination. These were also implemented in 2D but then in a plane through the thickness of the laminate (the $(x,z)$-plane) [19,20]. The 2D case in the $(x,y)$-plane is more challenging, because it calls for representation of a crack front rather than of a crack tip. From earlier work, it is known that in some cases with extensive delamination neglecting out-of-plane deformations has only a small influence on the global response [8]. Therefore the current 2D approach is of practical use. Additionally, in Section 7, a 2D model for the $(x,z)$-plane will be introduced to illustrate how out-of-plane variations, and hence the third dimension, can be added.

## 2. Cracked laminate model

In this section the model with given crack location is introduced. The crack location is described implicitly with a level set field $\phi$. It is of high practical use in level set methods to define the level set field as the signed distance function to the front $\Gamma$ [31], i.e. as

$$|\nabla\phi| = 1 \qquad \text{on } \Omega \tag{1}$$

$$\phi = 0 \qquad \text{on } \Gamma \tag{2}$$

In the Section 3, it will be outlined how $\phi$ evolves in time. For now we assume it to be given, and use it to distinguish between cracked and uncracked subdomains and to describe the front location. The laminate is delaminated where $\phi > 0$ and intact where $\phi < 0$. Hence, the crack front is located where $\phi = 0$ (see Fig. 1).

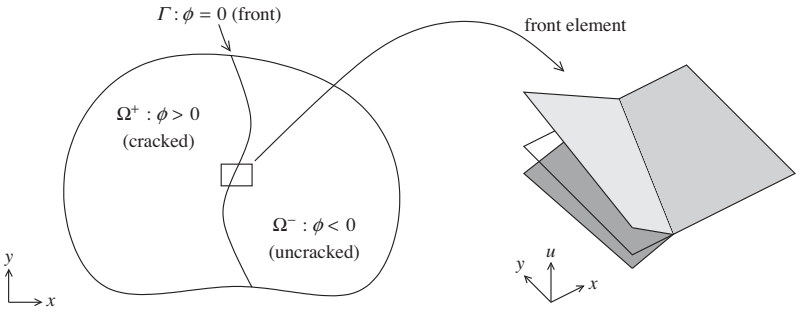


**Fig. 1.** Implicit definition of crack front with level set field $\phi$ and schematic deformation of quadrilateral element containing the crack front.

### 2.1. Kinematics

Away from the front, implementation of the delamination model is straightforward: on the cracked side there are two layers of elements that are not connected, and on the uncracked side there is a single layer of elements that represents the intact laminate. In the elements that are cut by the front, however, a non-standard formulation is required. The fundamental case that should be represented exactly consists of three different constant strain fields, one on the uncracked side and two on the cracked side. At the location of the delamination front, a jump in strain, or a weak discontinuity in the displacements, must be accommodated. More precisely, a pair of weak discontinuities must be embedded in the element formulation, one for each of the two sublaminates (top and bottom).

Modeling weak discontinuities with level sets can be done by enriching the finite element basis with special functions that have a discontinuity in the derivative exactly where $\phi = 0$ (see e.g. [32,33]). In the present case, however, this does not work. One could define two weakly discontinuous fields, one for the top part of the laminate, and one for the bottom part, as Fig. 2a. Two fields $u_{\text{top}}$ and $u_{\text{bot}}$ are depicted that both have a discontinuity in the derivative at $\Gamma$. For the present purpose, these two fields would have to be linked such that on one side of $\Gamma$ they are equal $\left(u^-_{\text{top}} = u^-_{\text{bot}}\right)$, while on the other side they are not $\left(u^+_{\text{top}} \neq u^+_{\text{bot}}\right)$. With the enrichment functions from literature [32,33] this cannot be achieved, because all basis functions in such an element are defined over the whole element domain. This makes it impossible to isolate the displacement field on one side of the front $\left(u^-_{\text{top}} = u^-_{\text{bot}} \leftrightarrow u^+_{\text{top}} = u^+_{\text{bot}}\right)$.

When, alternatively, both fields are defined with a strong discontinuity at $\Gamma$ either with Heaviside enrichment [9] or with duplicate nodes [34] the constraint $u^-_{\text{top}} = u^-_{\text{top}}$ can be easily achieved—in fact, it is possible to define only one field in $\Omega^-$, which we will henceforth refer to as $u^-$. In this formulation, jumps may appear in the displacement fields, annotated as $[\![u_{\text{top}}]\!]$ and $[\![u_{\text{bot}}]\!]$ in Fig. 2b. These jumps then have to be constrained. One way to do this is with Lagrange multipliers, in which case one has to be careful in defining the Lagrange multiplier space [35]. Another option is to use Nitsche's method [36,37]. A third alternative is to use a traction formulation earlier used in cohesive modeling in the context of X-FEM [38,39]. In Section 6.1 performance of the three methods will be compared, therefore the numerical formulation of all will be introduced here. But first, the kinematic formulation with strong discontinuities will be specified.

The complete displacement field consists of three independent vector fields, $\mathbf{u}_{\text{top}}{}^+$,$\mathbf{u}_{\text{bot}}{}^+$ and $\mathbf{u}^-$. In 3D they would all be defined on separate domains. In 2D, however, the two fields $\mathbf{u}_{\text{top}}{}^+$ and $\mathbf{u}_{\text{bot}}{}^+$ are both defined on the same domain. Integration through the thickness is implicit, in the sense that integrals are evaluated as:

$$\int_\Omega f \, \mathrm{d}\Omega = t_{\text{top}} \int_{\overline{\Omega}} f_{\text{top}} \, \mathrm{d}x \, \mathrm{d}y + t_{\text{bot}} \int_{\overline{\Omega}} f_{\text{bot}} \, \mathrm{d}x \, \mathrm{d}y \tag{3}$$

and

$$\int_\Gamma g \, \mathrm{d}\Gamma = t_{\text{top}} \int_{\overline{\Gamma}} g_{\text{top}} \, \mathrm{d}s + t_{\text{bot}} \int_{\overline{\Gamma}} g_{\text{bot}} \, \mathrm{d}s \tag{4}$$

where $\overline{\Gamma}$ and $\overline{\Omega}$ are the projections of the volume and surface domains $\Omega$ and $\Gamma$ on the plane of the laminate, $t_{\text{top}}$ and $t_{\text{bot}}$ are the thickness of the top and bottom parts, and $s$ is the parametrization of the front in the plane of the laminate.

For the discretized displacement field, we use Hansbo and Hansbo's method [34]. The top and bottom displacement fields are discretized as:

$$\begin{aligned} \mathbf{u}_{\text{top}} &= \begin{cases} \mathbf{N} \cdot \mathbf{d}^+_{\text{top}} & \mathbf{x} \in \Omega^+ \\ \mathbf{N} \cdot \mathbf{d}^- & \mathbf{x} \in \Omega^- \end{cases} \\ \mathbf{u}_{\text{bot}} &= \begin{cases} \mathbf{N} \cdot \mathbf{d}^+_{\text{bot}} & \mathbf{x} \in \Omega^+ \\ \mathbf{N} \cdot \mathbf{d}^- & \mathbf{x} \in \Omega^- \end{cases} \end{aligned} \tag{5}$$

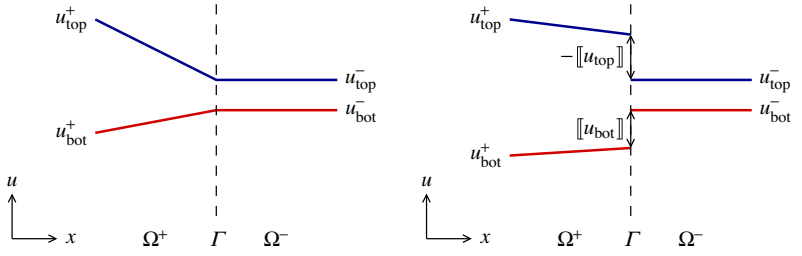


(a)Weak discontinuities (b)Strong discontinuities

**Fig. 2.** Two weakly discontinuous 1D fields $u_{\text{top}}$ and $u_{\text{bot}}$ and two strongly discontinuous fields with displacement jumps $[\![u_{\text{top}}]\!]$ and $[\![u_{\text{bot}}]\!]$ (right).

where **d** are nodal displacement values and **N** is the shape function matrix that relates the nodal values to the vector field. This means that in the elements that are completely in the cracked subdomain there are two layers of nodes and elements, while in elements that contain the crack front there are three layers of nodes and elements (see Fig. 3). Compatibility between $\mathbf{u}_{\text{top}}$ and $\mathbf{u}_{\text{bot}}$ is easily achieved by defining a single displacement field in $\Omega^-$.

When the front moves, the set of elements that contains the crack front may change and the mesh topology around the front must be updated. Each element that starts as uncracked may at some point during the analysis be crossed by the crack front, during which time the element is replaced with a triplet of elements: two for the uncracked side and one for the cracked side. After the crack front has passed through the entire element domain, a pair of elements remains, each with the same shape and area as the original element but with a different thickness.

Subtriangulation is used to evaluate integrals over the cracked elements. This means that the location of integration points changes when the front moves through an element. This is not problematic as long as linear elasticity is assumed for the bulk material. However, with a nonlinear material law, transfer of history variables will be necessary, or, alternatively, storage of history variables at the nodes. Integrals over the crack front are evaluated with two Gausspoints per cut element.

When the $\phi = 0$ line is very close to a node, it is assumed to cross the node exactly. The location of the front is moved to the node when $|\phi| \leqslant ch$, where in this work the constant $c$ is set to 0.01. The characteristic element size $h$ is in this paper defined as the length of the diagonal of the smallest rectangle around an element:

$$h = \min_{ie=1}^{nel} \left( \sqrt{\Delta x_{ie} \Delta y_{ie}} \right) \tag{6}$$

The kinematic formulation in Eq. (5) allows for a jump in the displacement field, which has to be closed. In the remainder of this section, different formulations will be introduced, and the complete finite element formulation will be derived for each of those.

### 2.2. Lagrange multipliers

The first method to close the gap is to make use of Lagrange multipliers. A second vector field $\boldsymbol{\lambda}$ is introduced in the potential energy of the system, which (neglecting body forces) is written as:

$$\Pi(\mathbf{u}, \boldsymbol{\lambda}) = \int_\Omega \psi(\nabla_s \mathbf{u}) \, \mathrm{d}\Omega + \int_\Gamma \boldsymbol{\lambda} \cdot [\![\mathbf{u}]\!] \, \mathrm{d}\Gamma - \int_{\Gamma_N} \mathbf{u} \cdot \mathbf{t}_N \, \mathrm{d}\Gamma \tag{7}$$

where $\psi(\nabla_s \mathbf{u})$ is the strain energy density and $\boldsymbol{\lambda}$ and $\mathbf{u}$ are the primary vector fields. $\Gamma_N$ is the part of the boundary on which Neumann boundary conditions are applied with traction $\mathbf{t}_N$. Note that with Eq. (4), there are in fact two Lagrange multiplier vector fields, one related to the top sublaminate and the other related to the bottom sublaminate.

This leads to the following variational formulation that will be discretized and solved:

$$\delta\Pi(\mathbf{u}, \boldsymbol{\lambda}, \delta\mathbf{u}, \delta\boldsymbol{\lambda}) = \int_\Omega \nabla_s \delta\mathbf{u} : \boldsymbol{\sigma} \, \mathrm{d}\Omega + \int_\Gamma [\![\delta\mathbf{u}]\!] \cdot \boldsymbol{\lambda} \, \mathrm{d}\Gamma + \int_\Gamma \delta\boldsymbol{\lambda} \cdot [\![\mathbf{u}]\!] \, \mathrm{d}\Gamma - \int_{\Gamma_N} \delta\mathbf{u} \cdot \mathbf{t}_N = 0 \tag{8}$$

where $\boldsymbol{\sigma} = \partial\psi / \partial(\nabla_s \mathbf{u})$.

There is a difficulty concerning the discretization of the Lagrange multiplier field. The value is only meaningful on the surface $\Gamma$, while this surface is not meshed. The most intuitive choice is to define degrees of freedom related to the Lagrange multiplier fields on the nodes of the set of elements that contain the front. However, this choice has proven to be unstable [40,41]. However, this can be solved by constraining the Lagrange multiplier space as proposed by Béchet et al. [35]. The idea is that variations in the Lagrange multiplier field normal to the surface are eliminated. This is done by tying the degrees of freedom related to node pairs that are connected across the front as illustrated in Fig. 4.

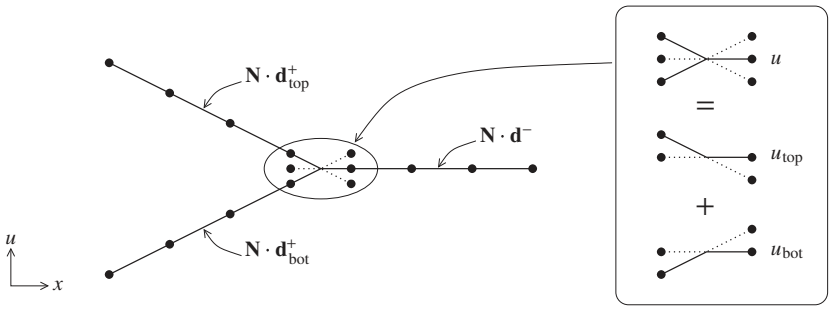


**Fig. 3.** One-dimensional representation of discretization with duplicate nodes. On the uncracked side there is one layer of elements while on the cracked side there are two, except in the element that contains the crack front, where there are three overlapping elements: one for the uncracked side and two for the cracked side.

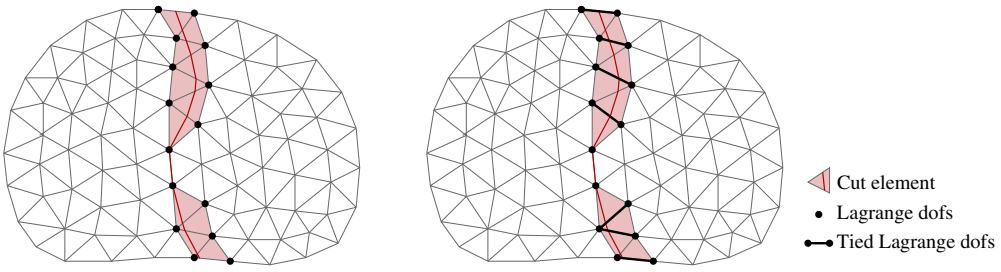


**Fig. 4.** Lagrange multiplier space: intuitive definition (left) and stabilized version (right).

The space is built in a variation to the algorithm by Béchet et al. [35]. The algorithm is such that the resulting space satisfies the following rules:

1. Nodes that are on the front remain untied.
2. All other nodes are connected to at least one node on the other side of the front.
3. It is not possible to remove a single tie without violating rule #2.

Generally, more than one space can be constructed that satisfy these three rules. Which of these is actualized depends on the quasi-random element numbering.

For second order elements, the degree of freedom related to the mid-nodes in cut elements is eliminated (assuming linear interpolation on the element boundary) except on the element boundary that is not cut. This means that there is one quadratic term in the basis for each cut element. However, if the length of the cut through an element is small with respect to the element size ($\Delta s \leqslant 0.1h$), this quadratic term is also eliminated.

We now discretize the primary fields and their variations as:

$$\begin{aligned} \mathbf{u} &= \mathbf{N}\cdot\mathbf{d} \quad \delta\mathbf{u} = \mathbf{N}\cdot\delta\mathbf{d} \\ \boldsymbol{\lambda} &= \mathbf{N}\cdot\mathbf{l} \quad \delta\boldsymbol{\lambda} = \mathbf{N}\cdot\delta\mathbf{l} \end{aligned} \tag{9}$$

With Eqs. (8) and (9), the discretized set of equations becomes:

$$\begin{bmatrix} \mathbf{K}_\Omega^- & \mathbf{0} & \mathbf{K}_\lambda \\ \mathbf{0} & \mathbf{K}_\Omega^+ & -\mathbf{K}_\lambda \\ \mathbf{K}_\lambda & -\mathbf{K}_\lambda & \mathbf{0} \end{bmatrix} \cdot \begin{bmatrix} \mathbf{d}^- \\ \mathbf{d}^+ \\ \mathbf{l} \end{bmatrix} = \begin{bmatrix} \mathbf{f}^- \\ \mathbf{f}^+ \\ \mathbf{0} \end{bmatrix} \tag{10}$$

with

$$\mathbf{K}_\Omega^\pm = \int_{\Omega^\pm} \nabla_s \mathbf{N}^T : \mathbb{C} : \nabla_s \mathbf{N} \, \mathrm{d}\Omega \tag{11}$$

$$\mathbf{K}_\lambda = \int_\Gamma \mathbf{N}^T \cdot \mathbf{N} \, \mathrm{d}\Gamma \tag{12}$$

$$\mathbf{f}^\pm = \int_{\Gamma_N^\pm} \mathbf{N}^T \cdot \mathbf{t}_N \, \mathrm{d}\Gamma \tag{13}$$

where $\mathbb{C} = \partial\boldsymbol{\sigma}/\partial(\nabla_s\mathbf{u})$. In this notation, $\mathbf{K}_\lambda$ is square and $\mathbf{d}^-$,$\mathbf{d}^+$ and $\mathbf{l}$ have equal lengths. In the implementation this is not the case, but for notational simplicity, it is here formulated as if $\mathbf{u}^+$,$\mathbf{u}^-$ and $\boldsymbol{\lambda}$ are discretized all over $\Omega$.

### *2.3. Nitsche's method*

Another way to close the gap is with Nitsche's method [36,37]. Here, two new terms are added to the potential (cf. Eq. (7)):

$$\Pi(\mathbf{u}) = \int_\Omega \psi(\nabla_s\mathbf{u}) \, \mathrm{d}\Omega + \int_\Gamma [\![u]\!] \cdot \langle \boldsymbol{\sigma}\cdot\mathbf{n}\rangle_\beta \, \mathrm{d}\Gamma + \frac{1}{2}\theta \int_\Gamma [\![\mathbf{u}]\!]\cdot[\![\mathbf{u}]\!] \, \mathrm{d}\Gamma - \int_{\Gamma_N} \mathbf{u}\cdot\mathbf{t}_N \, \mathrm{d}\Gamma \tag{14}$$

The first additional term already closes the gap in simple cases, but the second additional term is needed to stabilize the solution, where $\theta$ is a penalty parameter. The variational form is:

$$\begin{aligned} \delta\Pi(\mathbf{u},\delta\mathbf{u}) = &\int_\Omega \nabla_s\delta\mathbf{u} : \boldsymbol{\sigma} \, \mathrm{d}\Omega + \int_\Gamma \langle \mathbf{n}\cdot\mathbb{C} : \nabla_s\delta\mathbf{u}\rangle_\beta \cdot [\![\mathbf{u}]\!] \, \mathrm{d}\Gamma + \int_\Gamma [\![\delta\mathbf{u}]\!]\cdot\langle\boldsymbol{\sigma}\cdot\mathbf{n}\rangle_\beta + \theta\int_\Gamma [\![\delta\mathbf{u}]\!]\cdot[\![\mathbf{u}]\!] \, \mathrm{d}\Gamma - \int_{\Gamma_N}\delta\mathbf{u}\cdot\mathbf{t}_N \\ &= 0 \end{aligned} \tag{15}$$

The brackets in the first additional term of Eq. (14) indicate that the stress value has to be related to the two values of the stress that are available on both sides of the discontinuity:

$$\langle \boldsymbol{\sigma} \cdot \mathbf{n} \rangle_\beta = \beta(\boldsymbol{\sigma}^+ \cdot \mathbf{n}) + (1-\beta)(\boldsymbol{\sigma}^- \cdot \mathbf{n}) \tag{16}$$

where $\mathbf{n}$ is the normal vector to the plane over which the discontinuity is defined. According to Mergheim and Steinmann [36] it is best to choose $\beta$ equal to 1 or 0 depending on the location of the discontinuity in the element, such that the stress from the larger sub-element is used, but for simplicity, Mergheim et al. use an average value with $\beta = 1/2$, as do Dolbow and Hariri [37]. In the current work, however, $\boldsymbol{\sigma} \cdot \mathbf{n}$ is not continuous over $\Gamma$. The idea behind Nitsche's method is that for a zero jump, the $\boldsymbol{\sigma} \cdot \mathbf{n}$ term adds a traction on the face of the discontinuity that is in equilibrium with the neighboring stress. Therefore, the solution with zero crack opening is the equilibrium solution. In the delamination model, the equilibrium relation that should be satisfied over the discontinuity is:

$$t_{\text{bot}}(\boldsymbol{\sigma}^+_{\text{bot}} \cdot \mathbf{n}) + t_{\text{top}}\left(\boldsymbol{\sigma}^+_{\text{top}} \cdot \mathbf{n}\right) = t_{\text{bot}}(\boldsymbol{\sigma}^-_{\text{bot}} \cdot \mathbf{n}) + t_{\text{top}}\left(\boldsymbol{\sigma}^-_{\text{top}} \cdot \mathbf{n}\right) \tag{17}$$

For the cracked part, the traction that is added on the face should be in equilibrium with the stress in the neighboring material, but for the uncracked part, this only needs to hold after summation through the thickness. Therefore, $\beta$ must be set to 1. This is not good for the stability of the method, because the minimum value of $\theta$ that is required for stability is inversely dependent on the size of the smallest cut element.

The discretized set of equations is:

$$\begin{bmatrix} \mathbf{K}^-_\Omega + \mathbf{K}_\theta & \mathbf{K}_\sigma - \mathbf{K}_\theta \\ \mathbf{K}^T_\sigma - \mathbf{K}_\theta & \mathbf{K}^+_\Omega - \mathbf{K}_\sigma - \mathbf{K}^T_\sigma + \mathbf{K}_\theta \end{bmatrix} \cdot \begin{bmatrix} \mathbf{d}^- \\ \mathbf{d}^+ \end{bmatrix} = \begin{bmatrix} \mathbf{f}^- \\ \mathbf{f}^+ \end{bmatrix} \tag{18}$$

with

$$\mathbf{K}_\sigma = \int_\Gamma \mathbf{N}^T \cdot (\mathbb{C} : \nabla_s \mathbf{N} \cdot \mathbf{n}) \, \mathrm{d}\Gamma \tag{19}$$

$$\mathbf{K}_\theta = \theta \int_\Gamma \mathbf{N}^T \cdot \mathbf{N} \, \mathrm{d}\Gamma \tag{20}$$

### *2.4. Equilibrating traction*

A third way to close the gap is by using an internal traction on $\Gamma$ that is directly related to the neighboring stress. When an internal traction on the crack faces is added, the potential becomes:

$$\Pi(\mathbf{u}) = \int_\Omega \psi(\nabla_s \mathbf{u}) \, \mathrm{d}\Omega + \int_\Gamma [\![u]\!] \cdot \mathbf{t}, \mathrm{d}\Gamma - \int_{\Gamma_N} \mathbf{u} \cdot \mathbf{t}_N \, \mathrm{d}\Gamma \tag{21}$$

And the variational form is:

$$\delta\Pi(\mathbf{u}, \delta\mathbf{u}) = \int_\Omega \nabla_s \delta\mathbf{u} : \boldsymbol{\sigma} \, \mathrm{d}\Omega + \int_\Gamma [\![\delta\mathbf{u}]\!] \cdot \mathbf{t} \, \mathrm{d}\Gamma - \int_{\Gamma_N} \delta\mathbf{u} \cdot \mathbf{t}_N = 0 \tag{22}$$

Then, in order to let the traction close the gap effectively, $\mathbf{t}$ is made to depend on $\mathbf{u}$ as:

$$\mathbf{t} = (\boldsymbol{\sigma}^+ \cdot \mathbf{n}) + \theta [\![\mathbf{u}]\!] \tag{23}$$

This is similar to earlier formulations in the context of cohesive cracking [38,39], except that again the stress $\sigma^+$ is taken instead of the average of $\sigma^+$ and $\sigma^-$ and that there is no possibility of damage. With this definition of $\mathbf{t}$ and nonzero $\theta$, equilibrium is satisfied if and only if the gap is closed $[\![\mathbf{u}]\!] = \mathbf{0}$. Substitution into Eq. (22) gives:

$$\int_\Omega \nabla_s \delta\mathbf{u} : \boldsymbol{\sigma} \, \mathrm{d}\Omega + \int_\Gamma [\![\delta\mathbf{u}]\!] \cdot (\boldsymbol{\sigma}^+ \cdot \mathbf{n}) + \theta \int_\Gamma [\![\delta\mathbf{u}]\!] \cdot [\![\mathbf{u}]\!] \, \mathrm{d}\Gamma - \int_{\Gamma_N} \delta\mathbf{u} \cdot \mathbf{t}_N = 0 \tag{24}$$

This is less mathematically rigorous, because in going from Eq. (21) to Eq. (22) we assumed $\mathbf{t}$ to be independent of $\mathbf{u}$. Therefore, in fact, the weak form Eq. (24) can no longer be traced back to the potential Eq. (21), with loss of symmetry as a consequence. Nevertheless, this is still an equilibrium relation with a unique solution that satisfies $[\![\mathbf{u}]\!] = \mathbf{0}$. The resulting system of equations is very similar to that in Eq. (18) except that the $\mathbf{K}^T_\sigma$ terms are missing:

$$\begin{bmatrix} \mathbf{K}^-_\Omega + \mathbf{K}_\theta & \mathbf{K}_\sigma - \mathbf{K}_\theta \\ -\mathbf{K}_\theta & \mathbf{K}^+_\Omega - \mathbf{K}_\sigma + \mathbf{K}_\theta \end{bmatrix} \cdot \begin{bmatrix} \mathbf{d}^- \\ \mathbf{d}^+ \end{bmatrix} = \begin{bmatrix} \mathbf{f}^- \\ \mathbf{f}^+ \end{bmatrix} \tag{25}$$

### *2.5. Augmented Lagrange*

Finally, it is possible to combine the Lagrange multipliers with a penalty term. The potential is then defined as (cf. Eqs. (7) and (14))

$$\Pi(\mathbf{u},\boldsymbol{\lambda}) = \int_\Omega \psi(\nabla_s \mathbf{u})\ \mathrm{d}\Omega + \int_\Gamma \boldsymbol{\lambda}\cdot[\![\mathbf{u}]\!]\ \mathrm{d}\Gamma + \frac{1}{2}\theta\int_\Gamma [\![\mathbf{u}]\!]\cdot[\![\mathbf{u}]\!]\ \mathrm{d}\Gamma - \int_{\Gamma_N}\mathbf{u}\cdot\mathbf{t}_N\ \mathrm{d}\Gamma \tag{26}$$

It follows from the previous considerations that the system of equations in this case is:

$$\begin{bmatrix} \mathbf{K}_\Omega^- + \mathbf{K}_\theta & -\mathbf{K}_\theta & \mathbf{K}_\lambda \\ -\mathbf{K}_\theta & \mathbf{K}_\Omega^+ + \mathbf{K}_\theta & -\mathbf{K}_\lambda \\ \mathbf{K}_\lambda & -\mathbf{K}_\lambda & \mathbf{0} \end{bmatrix} \cdot \begin{bmatrix} \mathbf{d}^- \\ \mathbf{d}^+ \\ \mathbf{l} \end{bmatrix} = \begin{bmatrix} \mathbf{f}^- \\ \mathbf{f}^+ \\ \mathbf{0} \end{bmatrix} \tag{27}$$

The accuracy of the different gap closure methods that have been presented here will be assessed in Section 6.1.

## 3. Crack growth model

The model described in the previous section allows for mechanical analysis of a partially delaminated structure, where the delamination front can be arbitrarily located. Now we move on to a method with which this crack grows. Without cohesive zone, the crack necessarily grows according to the principle of fracture mechanics, i.e. growth occurs if the energy release upon crack growth is higher than the energy needed to form the additional crack surface. This is done in an explicit framework, which means that the difference between the current energy release $G$ and the critical energy release $G_c$ determines the velocity of the crack front (see Fig. 5). Obviously, $G$ can vary along the crack front, and as such the velocity is a function of the location on the front, which is denoted $s$. A simple expression is used to compute the normal velocity $v_n$:

$$v_n(s) = \frac{1}{\mu}\left\langle \frac{G(s)}{G_c} - 1 \right\rangle_+ \tag{28}$$

where $\mu$ is a constant that can be interpreted as a viscous resistance against crack growth. Brackets are used to denote the positivity condition $\langle\bullet\rangle_+ = (|\bullet| + \bullet)/2$, which reflects the irreversibility of crack growth.

In this section we will first develop the expression that is used to compute $G$ for a given front location and displacement field. Then the discretized form of Eq. (28) will be derived. Finally, it will be explained how this velocity is taken to update the level set field.

### 3.1. Energy release

As observed by Zou et al. [28] the use of laminate theory eliminates the stress singularity and introduces a discontinuity in the stress field that can be used as a configurational force for the crack growth. Laminate theory, or even shell theory, is not applied in a strict sense in this paper, but we do work from the assumption that higher order variations through the thickness are eliminated. Each of the displacement fields $\mathbf{u}^-$,$\mathbf{u}_{\text{top}}{}^+$ and $\mathbf{u}_{\text{bot}}{}^+$ is defined in 2D, without out-of-plane variations. In Section 7, linear variations of displacement will be introduced in each of the three fields. But it is fundamental for the presented method that through thickness variations are constrained as they typically are in plate, shell and laminate theories. In such a framework, the stress singularity around the front of a delamination crack cannot be represented and it is transformed into a jump in strain (and stress). Although our formulation differs from that by Zou et al. [28–30], we will also use this discontinuity to compute the energy release for crack growth.

For any transition from one state to another with a sharp front, the energy dissipation due to movement of that front $g$ can be expressed in terms of the jump in Eshelby tensor as [42]:

$$g = \mathbf{n}\cdot[\![\mathbf{P}]\!]\cdot\mathbf{n} \tag{29}$$

where $[\![\mathbf{P}]\!]$ is the jump in Eshelby tensor over the front, defined as:

$$[\![\mathbf{P}]\!] = \mathbf{P}^- - \mathbf{P}^+ \tag{30}$$

with

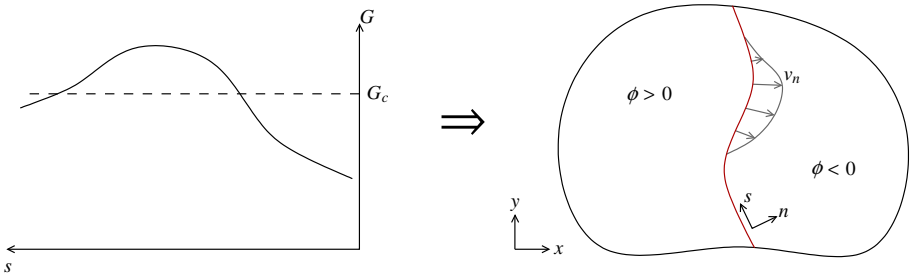


**Fig. 5.** Relation between energy release $G$ on the front and front velocity $v_n$.

$$\mathbf{P} = \psi\mathbf{I} - \nabla\mathbf{u}^T \cdot \boldsymbol{\sigma} \tag{31}$$

and, for linear elasticity:

$$\psi = \frac{1}{2}\nabla_s\mathbf{u} : \mathbb{C} : \nabla_s\mathbf{u} \tag{32}$$

Eq. (29) is valid for general surfaces in 3D. In the current case, although the crack front is a line, the discontinuity is defined over a surface through the thickness of the laminate. Therefore, in order to move from $g$, the energy release per unit area, to $G$, the energy release per unit crack front length, one needs to integrate $g$ over the thickness of the laminate:

$$G(s) = \int_t g(s,z)\ \mathrm{d}z \tag{33}$$

where $t$ is the thickness of the laminate. A similar expression for the energy release upon delamination crack growth has been used before by Nilsson and Storåkers [43] and Ousset [44].

This formulation is also applicable to problems with large displacements, as long as $\nabla\mathbf{u}$,$\boldsymbol{\sigma}$ and $\mathbf{n}$ are expressed in the current spatial configuration. Furthermore, any material law can be used that is derived from a potential $\psi$ such that $\boldsymbol{\sigma} = \partial\psi/\partial(\nabla_s\mathbf{u})$. For nonlinear materials, however, interpolation of the history variables or the stress will be necessary, because Eq. (29) is evaluated on the front, which is not where the history variables are stored.

### 3.2. Discretization

For the level set update, the velocity needs to be known at the nodes. However, $G$ is defined on the front. This is reminiscent of the formulation for the Lagrange multiplier in Section 2.2 where the field is also defined on $\Gamma$ and discretized on the nodes of the finite elements. In fact, the constrained space that has been introduced for the Lagrange multiplier (see Fig. 4) is the ideal basis for the normal velocity field.

Because the velocity degrees of freedom are then defined on the nodes, the field Eq. (28), which is defined on the front, cannot be imposed directly. Instead, a weak form is derived that is solved for the nodal velocities. First the velocity field is discretized with shape functions $\overline{\mathbf{N}}$ as $\overline{\mathbf{N}} \cdot \mathbf{v}_n$. Then it is imposed that Eq. (28) is satisfied in an integral sense after premultiplication with a set of test functions, for which the shape functions $\overline{\mathbf{N}}$ are chosen following Galerkin's method. The system of equations that is solved is then formulated as:

$$\mathbf{M} \cdot \mathbf{v}_n = \mathbf{f} \tag{34}$$

with

$$\mathbf{M} = \frac{\mu}{t}\int_\Gamma \overline{\mathbf{N}} \otimes \overline{\mathbf{N}}\ \mathrm{d}\Gamma \tag{35}$$

$$\mathbf{f} = \int_\Gamma \overline{\mathbf{N}}\left(\frac{\mathbf{n}\cdot[\![\mathbf{P}]\!]\cdot\mathbf{n}}{G_c} - \frac{1}{t}\right)\ \mathrm{d}\Gamma \tag{36}$$

The normal velocity $v_n$ is computed on the nodes of which the support is intersected by $\Gamma$, where ties between the nodal values are applied as in the Lagrange multiplier space. The thickness $t$ is introduced to cancel the integration through the thickness according to Eq. (4) on terms that are defined on $\overline{\Gamma}$ rather than on $\Gamma$. Note that the positivity condition has been removed; it will further on be reintroduced. Furthermore, the vector $\overline{\mathbf{N}}$ for scalar field $v_n$ is similar to but not the same as the matrix $\mathbf{N}$ for vector fields in Eq. (9). In the numerical examples presented in this work, first order triangular elements are used for discretization of the level set field $\phi$ and the normal velocity $v_n$ because this simplifies the fast marching algorithms, while second order elements are used for the discretization of the displacement and Lagrange multiplier fields because of their superior convergence properties.

However, to avoid oscillations on the front due to local inaccuracy in $G$, a diffusion term is added, after which Eq. (28) becomes:

$$v_n(s) + \frac{\kappa h^2}{\mu}\frac{\partial^2 v_n}{\partial s^2} = \frac{1}{\mu}\left\langle \frac{G(s)}{G_c} - 1 \right\rangle_+ \tag{37}$$

where $\kappa$ is a stabilization parameter and $h$ is the typical element size from Eq. (6). The element size $h$ is included here to make the stabilization term vanish upon mesh refinement.

The discretized set of Eq. (34) becomes:

$$[\mathbf{M} + \mathbf{K}] \cdot \mathbf{v}_n = \mathbf{f} \tag{38}$$

with

$$\mathbf{K} = \frac{\kappa h^2}{t}\int_\Gamma (\nabla\overline{\mathbf{N}}\cdot\mathbf{s}) \otimes (\nabla\overline{\mathbf{N}}\cdot\mathbf{s})\ \mathrm{d}\Gamma \tag{39}$$

### 3.3. Level set update

After solution of the system from Section 2, the system in Eq. (38) is solved to compute nodal velocity values around the front. In order to update the level set field which is defined over the whole domain $\Omega$, the velocity is extended. For this purpose, a fast marching method [31] is used. The set of nodes on which $v_n$ is defined as a degree of freedom is exactly the same as the set of nodes on which values are needed to initiate the fast marching method. The current level set values are used to sort the nodes on which the $v_n$ has not been solved, and to determine the order in which the nodes can be updated, marching away from the front. The nodal velocity is computed by solving the condition of normality between $\nabla\phi$ and $\nabla v_n$ on an element where two values of $v_n$ are known and one is unknown:

$$\nabla\phi \cdot \nabla v_n = 0 \tag{40}$$

Using the constant gradients of the standard interpolation functions on a triangle, this is a linear equation which can easily be solved for the unknown velocity value. If a node has multiple elements for which already two velocity values are known the value is taken from the element that is most normal to the level set, i.e. the element with the highest value for $|\nabla\phi \cdot \nabla N_i|$ where $i$ is the index of the node on which $v_n$ is unknown. In Fig. 6, the result of the velocity extension is visualized for a circular front.

Because the level set field is defined as a signed distance function, and the velocity field is defined as normal to the level sets, the update of the field with the obtained normal velocity field is very simple [45]. With forward Euler time discretization, the update is performed with:

$$\phi \leftarrow \phi + \langle v_n \rangle_+ \Delta t \tag{41}$$

where $\Delta t$ is the time step size. The brackets in Eq. (41) indicate that it is here that the positivity condition from Eq. (28) is imposed. For stability of the explicit level set update, $\Delta t$ is reduced when this is necessary to limit the growth of the front with more than half the element size per time step:

$$\Delta t = \min\left\{\Delta t^0, \frac{h}{2\max\{v_n\}}\right\} \tag{42}$$

where $\Delta t^0$ is the initial and maximum time step size. In combination with a loading scheme in which the displacement increment of the subsequent time step is adapted accordingly, it is possible to capture sharp load drops. The prescribed displacement value $u$ is updated with:

$$u \quad u + \Delta u^0 \frac{\Delta t}{\Delta t^0} \tag{43}$$

Hence the loading rate $\dot{u} = \Delta u^0/\Delta t^0$, which in interplay with the resistance parameter $\mu$ determines the viscosity of the crack. In the limit case where $\dot{u}\mu \to 0$, the quasi-static solution is obtained in which $G$ is not allowed to be larger than $G_c$. If $G$ becomes very high, $\Delta t$ will become very small, which results in an effective arrest of the increase in prescribed displacement during unstable crack growth.

Theoretically, if the normal velocity $v_n$ is defined on the front and extended to satisfy Eq. (40), and the level set field is a signed distance function satisfying Eq. (1), the level set field remains a signed distance function [45]. After discretization in time and space, however, the level set field may deviate from being an accurate representation of the signed-distance to the crack front. Therefore, occasional reinitialization of the level set field is necessary. This is also done with a fast marching method. Because it is a relatively cheap operation, it is performed every time step. The procedure is similar to that for the velocity extension, but this time the equation that is solved on the element is Eq. (1). With two known values of $\phi$ on

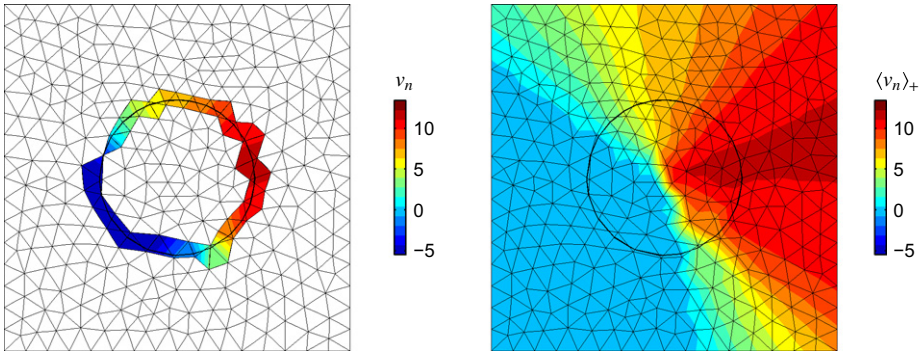


(a) After solving system of equations (38) (b) After extension and taking positive part

**Fig. 6.** Velocity field extension from a circular front.

the triangle this results in a quadratic equation which is solved for the unknown value, where the root with the maximum absolute value is chosen. If a node has multiple elements for which already two velocity values are known the value is taken from the element with the lowest value for $\max|\phi_j|,|\phi_k|$, where $j$ and $k$ are the indices of the nodes for which the level set value is known.

## 4. Initiation

Fracture mechanics models, such as the one described in the previous section, with their energy based failure criteria are generally not suitable for prediction of initiation of failure. However, for the proposed model it may be noticed that one can approach the limit case of an infinitesimal crack without problems. Consider the 2D version of a free edge delamination on a rectangular [0/90]-laminate. For this case, it can even be shown that, for a straight crack parallel to the free edge, $G$ is independent of the crack location. There are three strain fields, one for the uncracked part, and two for the cracked part; and each of these is independent of the exact crack location. We know (see Fig. 7) that the strain $\varepsilon_{xx}$ is equal to the applied strain everywhere, $\varepsilon_{xy}$ is equal to zero everywhere and for the three different values of $\varepsilon_{yy}$, we know that $\varepsilon^-_{yy}$ is such that $\sigma^-_{yy,\,\mathrm{bot}} = -\sigma^-_{yy,\mathrm{top}}$, $\sigma^+_{yy,\mathrm{bot}} = 0$ and $\sigma^+_{yy,\mathrm{top}} = 0$.

From this we infer, that even on an uncracked free edge, one can compute hypothetical strain fields for an infinitesimal crack. Generalizing to an $(n,s)$-frame aligned to an arbitrarily oriented free edge, the strain component $\varepsilon_{ss}$ in the cracked sublaminates will be the same as in the uncracked laminate, while the other strain components will be such that $\sigma_{nn} = \sigma_{ns} = 0$. With the constitutive law for the ply (or sublaminate) it is possible to compute the two unknown strain components $\varepsilon_{ns}$ and $\varepsilon_{nn}$, and subsequently the missing stress component $\sigma_{ss}$. This means hypothetical stress and strain tensors can be computed in the cracked sublaminates before a crack arises. With these, a hypothetical value for the component $P_{nn} = \mathbf{n}\cdot\mathbf{P}\cdot\mathbf{n}$ can be computed. $P_{nn}$ is defined as:

$$P_{nn} = \frac{1}{2}u_{i,j}\sigma_{ij} - \sigma_{nk}u_{k,n} \qquad (i,j,k) = (n,s) \tag{44}$$

It can be observed that the off-diagonal terms of $\nabla\mathbf{u}$ (which remain unknown) are all canceled by the zero off-diagonal terms of $\boldsymbol{\sigma}$. To be precise, Eq. (44) can be worked out for the cracked sublaminate near the free edge to:

$$P_{nn} = \frac{1}{2}u_{s,s}\sigma_{ss} \tag{45}$$

Therefore, we can compute the energy dissipation for crack growth from the free edge even in absence of an initial crack, and hence we can also use our energy criterion for initiation.

In terms of level set update, initiation also requires special treatment because we do not have a zero level set waiting on the boundary to be given a velocity. When the initiation criterion is met somewhere in an element along the free edge, a new zero level set is introduced in that element by setting the level set value its nodes which are on the boundary to $0.1h$. The signed distance function is updated accordingly where necessary.

As said in the beginning of this section, energy criteria are generally not useful for initiation. It is known from linear elastic fracture mechanics that the energy release for an infinitesimal crack in an uncracked body is equal to zero [46]. So one may wonder how it is possible that nonzero values are obtained in this case. The answer is this is due to assumptions of shell mechanics. Higher order variations in stress and strain through the thickness of the laminate are not modeled. Therefore, the influence of an infinitesimal crack is immediately felt through the thickness of the laminate. Obviously, this is not realistic. The stress field around the crack tip is not as simple as we assume. It is therefore reasonable to say that the assumptions of shell theory only start to be realistic when the crack length is several times more than the thickness of the laminate. Unstable initial crack growth, for instance, which can be expected when a crack nucleates along the free edge, will not be captured with this simplified approach.

Having said that, we observe that if one nevertheless makes the assumptions of shell theory even for infinitesimal cracks, this makes the initiation problem well-posed. Since we are mainly interested in large cracks, we take the inaccuracy in shell theory for small cracks for granted and make use of the observation that within the context of shell theory, an energy based

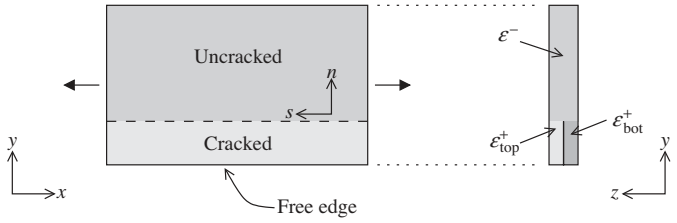


**Fig. 7.** Three strain fields in a 2D representation of rectangular laminate that is cracked from the free edge.

criterion can be used for crack initiation. One can say that the energy based criterion offers a reliable indicator for when the energy in the system is sufficient to let a crack propagate away from the free edge.

## 5. Global algorithm

**Box 1.**

Global algorithm for single time step.

1. Compute displacements for known crack front location
   - Assemble and solve linear elastic system (Eq. (25))
2. Grow cracks
   - Assemble and solve linear system for velocity on the front (Eq. (38))
   - Extend normal velocity (fast marching method, Eq. (40))
   - Update level set field (Eq. (41))
   - Check for initiation and update level set field if necessary
   - Reinitialize signed distance function (fast marching method, Eq. (1))
3. Go to next time step
   - Apply displacement increment with Eq. (43)

In Box 1, the global algorithm for a single time step is summarized. A staggered solution scheme is proposed. Firstly, the cracked laminate model with a given crack front location is solved for displacements with the X-FEM and a gap closure technique from Section 2. Secondly, crack growth is computed according to the relations in Section 3: the normal velocity on the front is computed, and the new crack front location is determined by updating the level set field. The check for initiation as described in Section 4 is performed near the end of the time step, before the reinitialization procedure.

It is emphasized that all operations in step 2 are relatively cheap in terms of computational effort. The linear system that is solved is of $O(\sqrt{n})$ where $n$ is the number of degrees of freedom in the linear system from step 1. Taken together, the operations in step 2 do not need the same computation time as the global solve in step 1. Therefore, the algorithm for a single time step is more efficient than that for cohesive methods, where the global solve is repeated several times per time step in an iterative algorithm. This gain in efficiency comes on top of the primary gain due to the possible increase in element size.

## 6. Numerical examples

### *6.1. Plate with circular hole: gap closure methods*

To investigate the different techniques from Section 2 for closing the gap in the cracked laminate model, a convergence analysis is performed on a [0/90]-laminate with a hole. Geometry and material parameters are taken from an analysis by Yang and Cox [5], which will be treated in more detail in Section 6.3. The thickness of the plies is 0.2 mm and elastic parameters are: $E_1 = 140 \times 10^3$ N mm$^{-2}$, $E_2 = 10 \times 10^3$ N mm$^{-2}$, $G_{12} = 5 \times 10^3$ N mm$^{-2}$ and $\nu_{12} = 0.21$. A quarter of the plate is modeled, and a uniform displacement is applied on the right boundary (see Fig. 8). A circular delamination of width 0.5 mm is placed around the front by setting the level set field to:

$$\phi(x, y) = 13.2 - \sqrt{x^2 + y^2} \tag{46}$$

The analysis is performed with different mesh densities around the delamination front; each time the error in $G$ is integrated numerically over the front with:

$$\epsilon = \frac{\int_{\bar{\Gamma}} |G - G_{\text{ref}}| \, \mathrm{d}s}{\int_{\bar{\Gamma}} |G_{\text{ref}}| \, \mathrm{d}s} \tag{47}$$

For the reference solution $G_{\text{ref}}$ results are taken from a fine mesh analysis in which the mesh is aligned with the front and the gap is closed with Lagrange multipliers. The integral in Eq. (47) is evaluated with the integration scheme on the non-aligned mesh, where the values of $G_{\text{ref}}$ are obtained through linear interpolation between values at the element mid-nodes, which are super-convergent points for the 6-node triangles that are used. In Fig. 9 convergence plots are shown. The fact that the convergence is not completely regular is related to the fact that the quality of the solution does not only depend on the element size, but also on how the elements are aligned with respect to the front. Nevertheless, clear trends can be observed.

Both Nitsche's method and the method of equilibrating traction outperform the Lagrange multiplier when the penalty parameter is chosen sufficiently high. Remarkably, the $\theta$-value for which the equilibrating traction gives a more accurate

$G$ than the Lagrange multiplier is two orders of magnitude higher than the value for which Nitsche's method is more accurate than the Lagrange multiplier.

When chosen sufficiently high, the penalty in the augmented Lagrangian method also improves the accuracy. For low values the influence of the penalty vanishes, which means that the results with standard Lagrange multipliers are obtained (it can be observed that the error from the augmented Lagrangian method with $\theta = 10^4$ is practically equal to the error with the standard Lagrangian method, which basically has $\theta = 0$).

For the following examples in this section, the traction method will be applied with $\theta = 10^7$.

### 6.2. Cracked shear lap

Next, a cracked shear lap is analyzed (see Fig. 10). A 0°-UD specimen with initial delamination is axially loaded, where the load is applied on only one of the two plies on the cracked side, such that the crack grows in mode II as a splitting phenomenon. With the assumption of neglecting out-of-plane deformations, the test is similar to the modified cracked shear lap test by Guimard et al. [48]. This is a relatively simple case with extensive delamination for which an exact solution exists. For the exact solution, the Poisson effect is neglected which makes the problem a 1D problem. The cracked parts and uncracked part are treated as trusses, with $\varepsilon^- = F/(E_1 wt), \varepsilon^+_{\text{top}} = F/(2E_1 wt)$ and $\varepsilon^+_{\text{bot}} = 0$. The displacement at the loaded end for given load $F$ and crack length $a$ is:

$$u = (l + a)\frac{F}{E_1 wt} \tag{48}$$

The potential energy of the system is:

$$\Pi = \frac{1}{2}\int_\Omega \varepsilon\sigma \, \mathrm{d}\Omega - Fu = -(l + a)\frac{F^2}{2E_1 wt} \tag{49}$$

The variation in potential energy upon crack growth is:

$$\delta\Pi = -\frac{F^2}{2E_1 wt}\delta a \tag{50}$$

Now, equating the loss in potential energy to the energy required to let the crack grow, yields the load for which the crack will grow:

$$\frac{F^2}{2E_1 wt}\delta a = G_c w \delta a \quad \Rightarrow \quad F = w\sqrt{2G_c E_1 t} \tag{51}$$

This case is analyzed numerically with the level set model. The same elastic parameters as in the previous example are used. The nonzero Poisson's ratio does not have a significant influence on the global energy in the system. A combination between a relatively low value of $\mu$ and a relatively low displacement rate is used: $\mu = 0.01$ s mm$^{-1}$ and $\dot{u} = 0.005$ mm s$^{-1}$, such that the quasi-static solution with $G \leqslant G_c$ is approached. Furthermore, we use a value of $\kappa = 0.1$ s mm$^{-1}$. In this way, the results can be compared with the 1D solution from Eq. (51) and with computational results obtained in a quasi-static framework with interface elements in which the cohesive zone is modeled.

The initial front is straight and located at 4 mm of the loaded edge. The evolution of the front is visualized in Fig. 11. It can be observed that the front does not remain straight, which is due to the nonzero Poisson's ratio. The movement of the front

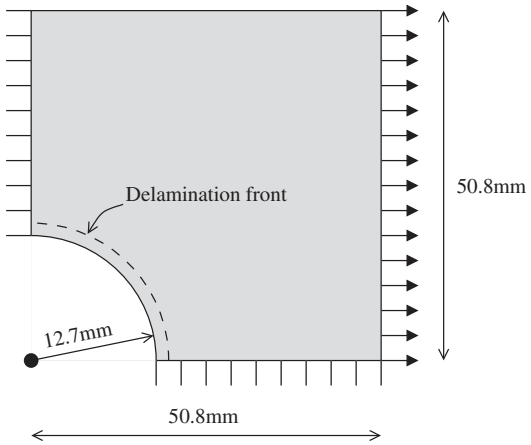


**Fig. 8.** Geometry of plate with circular hole and initial delamination front.

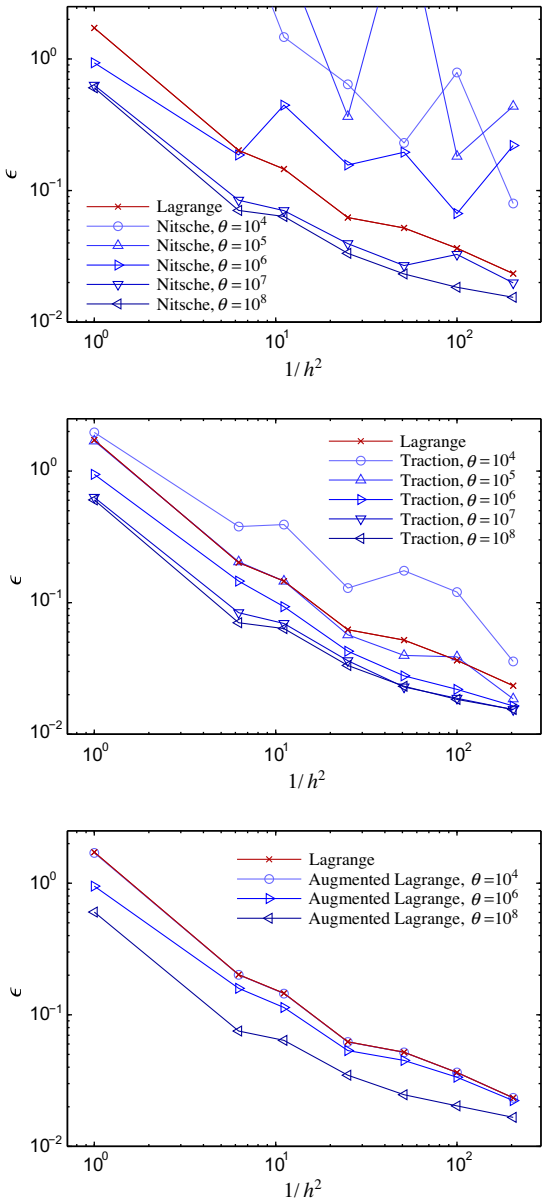


**Fig. 9.** Error in $G$ evaluated over the crack front for different crack closure methods ($h$ is not from Eq. (6) but from the input file for the mesh generator [47]).

through the domain is stable, even though a rather coarse mesh is used. In Fig. 12, the obtained load displacement data are compared with results from the quasi-static analysis with interface elements and a simple cohesive damage law as described in [8]. The results from the two analyses are very similar, and they are also in agreement with the theoretical finding that crack growth occurs at a constant load level. In the cohesive element analysis, a much finer discretization is required to get convergence of the nonlinear solver, even though the robust dissipation-based arc-length method with adaptive time stepping by Verhoosel et al. [49] is employed. Furthermore, the time steps are necessarily small. The difference in time step size between the two analyses can be observed in the right diagram of Fig. 12. Furthermore, the level set model requires only one linear solve for the elasticity problem per time step, while the computation with interface elements needs about four iterations in a successful time step and many more in time steps where convergence is not directly found and the step size has to be reduced. The total number of system solves in the iterative computation was 3871, versus a number of time steps in the level set computation of only 142.

The shape and location of the delamination front in the two analyses are also compared. Cohesive damage in the interface elements and the front location from the new approach are plotted for the same value of prescribed displacement in Fig. 13. The front in the level set analysis, falls within the cohesive zone from the nonlinear analysis. The discretization that is shown

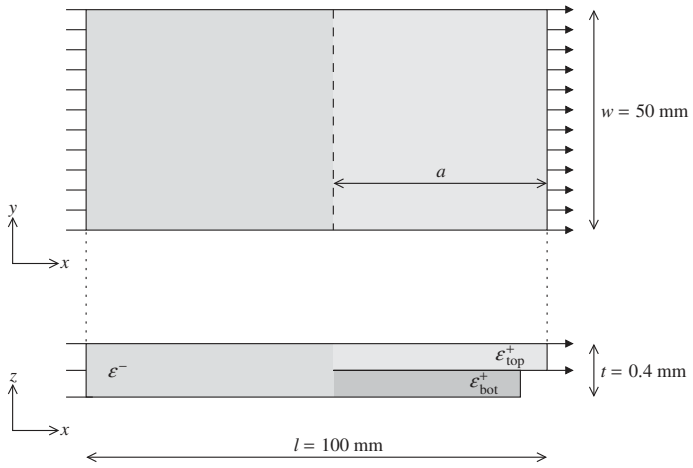


**Fig. 10.** Geometry of cracked shear lap.

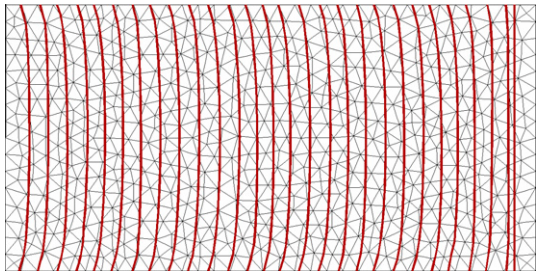

**Fig. 11.** Delamination growth in level set analysis of cracked shear lap; the front moves from right to left, it is depicted for intervals of 5 time steps.

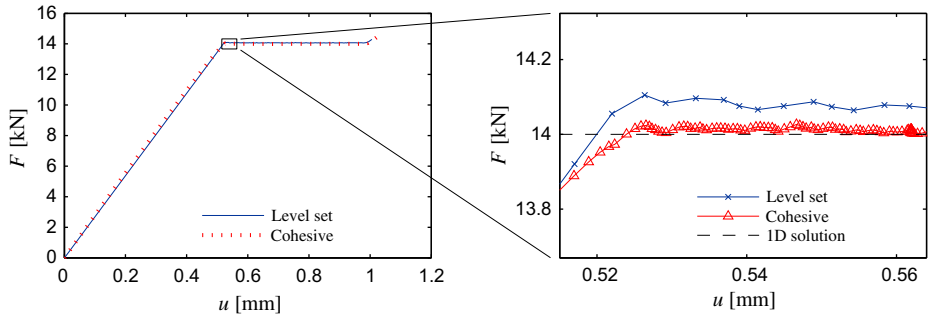


**Fig. 12.** Load-displacement results for 2D cracked shear lap with cohesive interface elements and the proposed level set method.

in this figure is the one that was used for the cohesive analysis, which was found to be the coarsest allowable mesh ($h \approx 1$ mm). The efficiency gain of the level set method is clear when this mesh is compared with the one used for the level set analysis in Fig. 11, although the contrast is amplified by the fact that linear elements were used in the cohesive analysis, versus quadratic elements in the level set analysis. The number of nodes in the cohesive analysis was 11,736, while for the level set analysis it grew from an initial number of 2775 to a final 5038. More important than the quantitative gain in this particular case is, however, that the required element size scales with the in-plane dimensions for the level set method, while it is constant for the cohesive approach. In other words, upon in-plane scaling with a factor $n$, the number of nodes required for the cohesive analysis scales with a factor $n^2$ while for the level set analysis, the number of nodes that is required remains the same. So if the specimen dimensions would be scaled up, the gain in efficiency would become larger and larger.

### *6.3. Plate with circular hole: initiation and non-self-similar crack growth*

Now a more challenging example is treated, with delamination growth that is not self-similar. The circular plate from Section 6.1 is analyzed without initial delamination. The same parameters are used as in the previous example. Again,

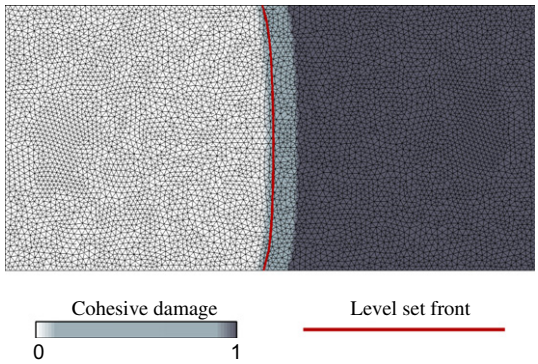


**Fig. 13.** Delamination damage in cohesive zone analysis for $u = 0.75$ mm with, superposed, delamination front location in level set analysis at the same displacement level.

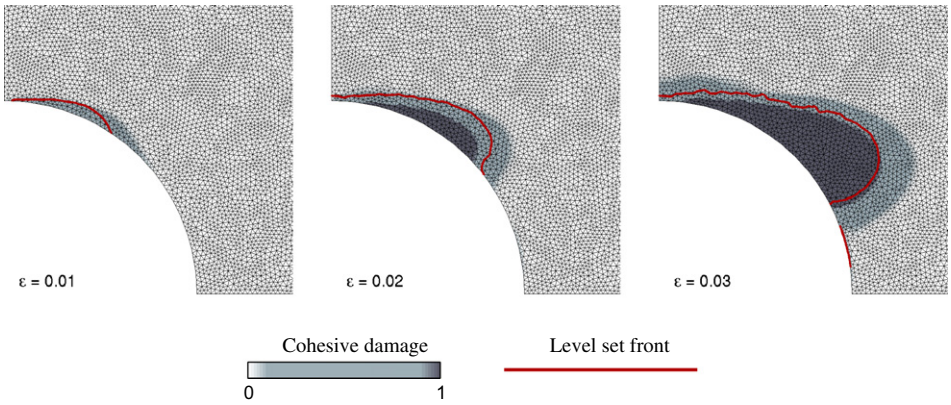


**Fig. 14.** Evolution of damage in cohesive zone analysis and evolution of front in level set analysis of plate with circular hole without initial delamination.

the analysis is performed with cohesive elements as well as with the proposed level set model, where the cohesive zone analysis is the same as that in Yang and Cox [5] except that we use a cohesive law with linear softening, and that our analysis is performed in 2D. There is no initial delamination, so this is also a test for the initiation model introduced in Section 4.

In Fig. 14 the crack growth for the two models is compared. Again, it can be observed that the front location predicted by the level set model falls within the cohesive zone as predicted by the interface elements. Initiation is predicted at the correct location. Moreover, the crack front is introduced timely: where it is inserted it starts growing straight away.

Furthermore, this example shows that the proposed energy release rate criterion is directly applicable to orthotropic materials. Although orthotropy is not explicitly present in Eq. (29), it is introduced via the dependence of the Eshelby tensor on the stress. With an isotropic material, there would be no delamination in this case.

## 7. Through thickness variations

The main point of this paper is to use level sets to describe the delamination front. In this way, the cohesive zone does not need to be resolved, but this requires a formulation for the configurational force to compute the energy release upon crack growth. In Section 3 it has been proposed to use the jump in Eshelby tensor in order to compute the energy release for movement of the crack front. One may wonder whether and how this concept can be generalized to full three dimensional modeling where stress and strain quantities may vary through the thickness of the laminate. To illustrate the potential of the configurational force for three dimensional analysis the configurational force concept is tested on several simple beam examples in this section. These analyses are again performed in 2D, but now in the $(x,z)$-plane. In this case there is no need for a level set field. The crack front becomes a crack tip, which can be located with its $x$-coordinate.

### *7.1. 2D model in the (x,z)-plane*

The element which contains the tip consists of a triplet of overlapping elements, each of which is only partially active. In the $(x,y)$-model, it was implicit that the weak discontinuity in the displacement field was applied through the thickness of

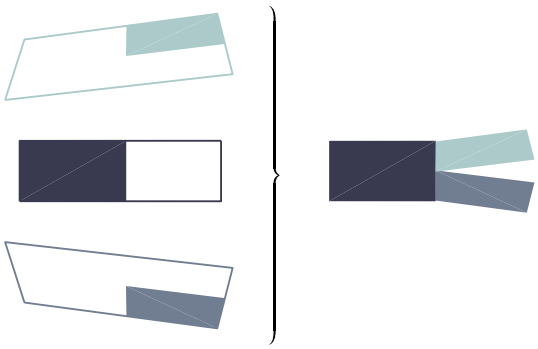

**Fig. 15.** Illustration of possible deformation of tip element as three partially active overlapping elements; on the left the outline of the three deformed elements, filled where they are active; on the right the composed deformation of the three active parts.

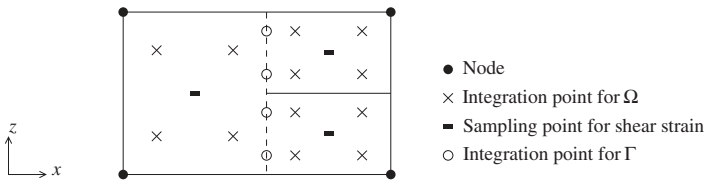


**Fig. 16.** Integration scheme for triplet of overlapping elements.

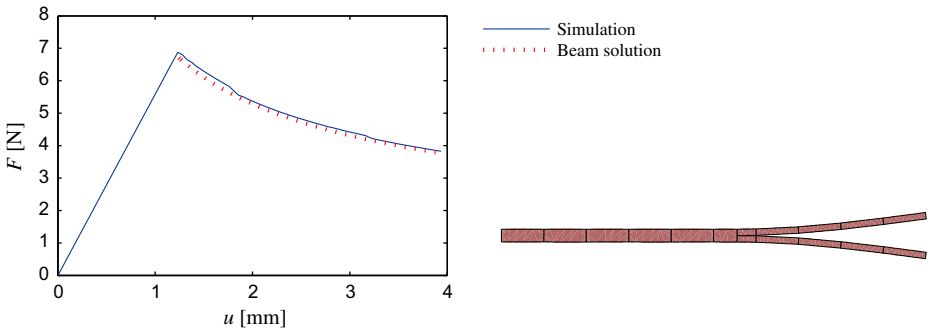


**Fig. 17.** Load-displacement diagram from double cantilever beam in comparison with analytical solution; the final deformation is also shown.

the laminate at the location of the front. Here the through-thickness nature of the weak discontinuity becomes explicit. In Fig. 15 a possible deformation of the tip element is illustrated as being composed of the deformation of three elements all of which are partially active. There is a strong discontinuity between the two parts on the cracked side and a weak discontinuity over the entire height of the element. In this image, inspired by the double cantilever beam test, the two elements that correspond with the cracked part display a bending deformation, while the element corresponding with the uncracked part is not deforming.

The integral over the thickness in Eq. (33) is now evaluated with two gauss points for the top part and two gauss points for the bottom part (see Fig. 16). Standard quadrilateral solid elements are used, with a selective reduced integration scheme to avoid shear locking. That is, the shear strain is evaluated at the element center, or, in the case of partially active elements, at the center of the active part. This element still displays Poisson thickness locking [50]. For three-dimensional modeling, a more suitable shell element will have to be used, but for the simple tests performed here, locking can be avoided without severe loss of accuracy by setting the Poisson's ratio in the solid element to zero.

Again Hansbo's method used to model the strong discontinuity and the weak discontinuities and Lagrange multipliers are used to close the gap on $\Gamma$. Four $\lambda_x$ degrees of freedom are defined through the thickness (two per sublaminate) as well as two $\lambda_z$ degrees of freedom (one per sublaminate).

### *7.2. Numerical examples in the (x,z)-plane*

As a first numerical example, a double cantilever beam is analyzed. Results are compared with the analytical solution derived from simple beam relations. The beam solution is given by:

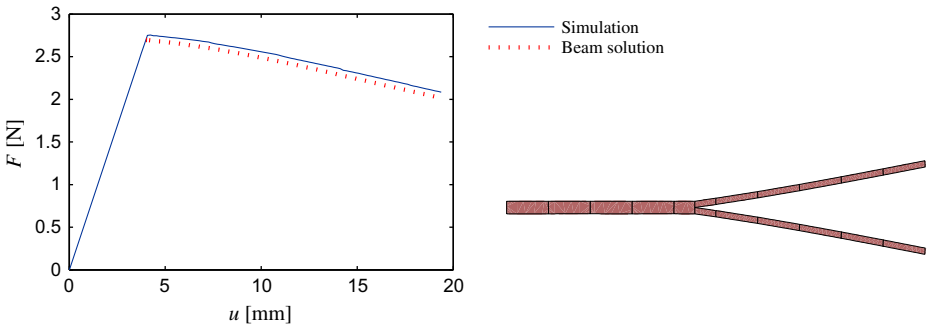


**Fig. 18.** Load-displacement diagram from shear deformable double cantilever beam in comparison with analytical solution; the final deformation is also shown.

$$u = \frac{32Fa^3}{Ewt^3} + \frac{2Fa}{G_{13}wt} \tag{52}$$

and

$$\frac{1}{2}wG_c = \frac{1}{2}F\frac{\partial u}{\partial a} \tag{53}$$

where $u$ is the end displacement of a single arm, $t$ is the height of the beam, $w$ is the unit depth, $a$ is the length of the crack, $E$ is the Young's modulus and $G_{13}$ is the shear modulus. In Eq. (52) a value of 1.0 is used for the Timoshenko shear correction factor, as it effectively is in the finite element. Furthermore, terms that can be added for deformation of the uncracked part (see Reeder and Crews [51]) are neglected, which is safe for a thin isotropic beam.

An isotropic material is used with $E = 100 \times 10^3$ N mm$^{-2}$ and $G_{13} = E/2$. The beam with a length of 100 mm and a height of 3 mm is discretized with elements that are 10 mm long. An initial notch with a length of 25 mm is placed at the mid-height of the beam. Furthermore, we use $G_c = 1$ N mm$^{-1}$, $\mu = 0.1$ s mm$^{-1}$ and $\dot{u} = 0.02$ mm s$^{-1}$. In Fig. 17 the obtained load–displacement curve is presented in comparison with the analytical beam solution. The final deformation is also visualized. It can be observed that although the discretization is extremely coarse, the numerical solution is close to the analytical solution.

It is emphasized that with the proposed method a smooth response is obtained for this case irrespective of the brittleness of the system or the size of the elements. Although this is a relatively simple case, cohesive analysis demands a fine mesh to obtain a load–displacement relation without spurious snap-backs. Smooth results have not been presented before with an element size comparable to that in Fig. 17. The advantage of the present method in comparison with existing enrichment schemes is that here the cohesive zone is eliminated altogether. The downside of eliminating the cohesive zone is that this does not lead to reasonable results in cases with ductile failure, i.e. in cases where the cohesive zone length is of the same order as the length of the specimen. For delamination in composite laminates, however, the length of the cohesive zone is typically very small with respect to in-plane dimensions of the laminate.

To show the generic validity of the configurational force, the test is repeated with a shear deformable beam where $G_{13}$ is set to $5 \times 10^3$ N mm$^{-2}$. The initial notch length is set to 11 mm, such that the initial part of the response is strongly shear dominated. Here the assumption that the uncracked part does not deform is not justified, but the same kinematic constraint is applied in the numerical model as in the beam model, so the comparison between beam solution and numerical results remains meaningful. Results are presented in Fig. 18. In the beginning the solution is close to the pure shear solution with constant load,[1] but as the crack grows the bending part becomes increasingly significant. The analytical solution is once again very accurately captured.

It is noted that in the analytical solution shear deformation of the uncracked part is not taken into account. This deformation is also prevented in the numerical model. Therefore, both solutions deviate equally from the more realistic full continuum solution. Notwithstanding this inaccuracy, the match between the two solutions shows that the jump in Eshelby tensor gives robust and sensible results for different cases in which a crack tip advances through very large elements.

Finally, the mode II case of end-notched flexure is analyzed. The same beam (with restored shear stiffness) is subjected to three-point bending. The initial notch length is set to 32 mm and the loading rate reduced to $\dot{u} = 0.003$ mm s $- 1$. The analytical solution is found with

$$u = \frac{F(l^3 + 12a^3)}{4Ewt^3} + \frac{Fl}{4G_{13}wt} \tag{54}$$

and

[1] The pure shear case with $G_{13} \ll E$ is mathematically equivalent to the 1D model of the cracked shear lap from Section 6.2.

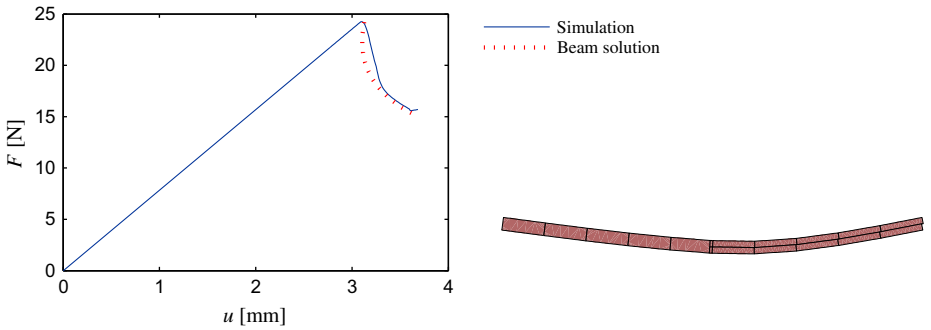


**Fig. 19.** Load-displacement diagram from end notched flexure test in comparison with analytical solution; the final deformation is also shown.

$$wG_c = \frac{1}{2} F \frac{\partial u}{\partial a} \tag{55}$$

where $l$ is half of the length of the beam. In Fig. 19 it can be observed that the initial part of the beam solution with unstable crack growth cannot be represented, which is due to the explicit crack growth law. But eventually the simulation results grow very close to the analytical solution, until the assumptions of the analytical solution lose their validity when the crack tip passes the half-span of the beam.

For these examples, the post peak response is governed by the fracture toughness. The agreement with analytical results therefore confirms that the local configurational force with the jump in Eshelby tensor is a correct measure for the energy release upon crack growth. The analyses are performed with extremely large elements, which confirms the potential of the proposed method for efficient simulations with large scale delamination.

## 8. Conclusions

In this paper a new approach to the computational modeling of delamination has been presented. The first main feature of the model is a new enrichment scheme for the displacement field of a partially cracked laminate. Weak discontinuities are inserted at the location of the crack front, where the level set method is employed to describe the front location such that it can intersect the elements at arbitrary locations. As a result, the kinematics are such that the laminate has a single displacement field on the uncracked side, and two independent displacement fields on the cracked side, while the interface between the cracked and uncracked subdomains is not necessarily aligned with the mesh. A smooth progression of the front through the finite elements is possible, which is crucial for the modeling of crack growth with large elements.

In order to achieve the weak discontinuity between two independent displacement fields on the cracked side and another displacement field on the uncracked side, a formulation for strong discontinuities is used in combination with a gap closure technique. Three different techniques to close the gap are investigated, Lagrange multipliers, Nitsche's method and an equilibrating traction. Concerning these, a small survey has shown that the third leads most easily to accurate results.

The second main feature of the model is a new way to compute the energy release for a delamination crack. The weak discontinuity in the displacement field results in a jump in strain (and stress) over the surface through the thickness of the laminate at the location of the crack front. It is this jump in strain that can then be used as configurational force after it is transformed into a jump in Eshelby tensor. The fact is used that the jump in Eshelby tensor over an interface (in this case the interface between uncracked and cracked parts) gives information on the energy that is released when this interface is moved (in this case, the energy release upon crack growth). The thus computed energy release is used to compute the crack velocity in an explicit crack growth law. This velocity is then used to update the level set field, and hence the crack location.

The assumptions of shell theory remove the stress singularity from the linear elastic displacement field around the crack front. Higher order variations in the stress field through the thickness of the laminate are removed and as such the stress singularity is transformed into a weak discontinuity over a plane through the thickness. Within the context of shell theory the solution with a weak discontinuity is the exact solution and therefore it converges to a unique solution without singularity upon in-plane refinement. Obviously, through-thickness refinement does not make sense within the context of plate mechanics and therefore the proposed method is only valid for thin structures where elimination of higher order variations through the thickness is admissible.

In several numerical examples it has been shown that the thus predicted delamination cracks are equal in shape and size to those computed with the well-established approach of using interface elements with a cohesive zone. This confirms the theory that the jump in Eshelby tensor in the proposed model is equal to the energy release for crack growth. While results are similar to those obtained in classical cohesive zone analysis, a threefold gain in efficiency is made: the elements can be larger, the time steps can be larger, and the number of system solves per time step is limited to one for the global system plus one for a smaller system.

A third issue that has been addressed in this publication is the initiation of new cracks. Generally, fracture mechanics models are not applicable without the presence of initial cracks. In this case, however, the energy based criterion can be used for prediction of crack initiation along the free edge. The energy release can be found for crack growth from the free edge, because stress and strain near the free edge after cracking can be computed from the strain of the uncracked body. The fact that the energy release is finite is a consequence of the assumptions of shell theory. The crack is initiated if the elastic energy near the free edge is sufficient to drive crack growth away from the free edge. For cases where delamination cracks eventually grow very large this is an adequate initiation criterion.

Several challenges remain open for future development of this method, the most obvious being the extension to three dimensional modeling with shell elements and large deformations. Furthermore, it is important to find a formulation for implicit update of the crack front and to be able to extract the pure mode contributions from the energy release rate, $G_I$, $G_{II}$ and $G_{III}$, in order to relate the fracture toughness $G_c$ to the ratio between those. Nevertheless, this paper already shows a more extensive capability of the current method than of existing enrichment schemes for using larger elements in delamination analysis. The fact that the cohesive zone is eliminated altogether opens the door to significant upscaling of model dimensions without excessive increase in computational cost.

## Acknowledgment

FPM and LJS acknowledge financial support by the Dutch Technology Foundation STW under Grant 06623.

## References

[1] Allix O, Ladevèze P. Interlaminar interface modelling for the prediction of delamination. Compos Struct 1992;22:235–42.
[2] Schellekens JCJ, de Borst R. Free edge delamination in carbon-epoxy laminates: a novel numerical/experimental approach. Compos Struct 1994;28:357–73.
[3] Alfano G, Crisfield MA. Finite element interface models for the delamination analysis of laminated composites: mechanical and computational issues. Int J Numer Method Eng 2001:1701–36.
[4] Camanho PP, Dávila CG, de Moura MF. Numerical simulation of mixed-mode progressive delamination in composite materials. J Compos Mater 2003;37:1415–38.
[5] Yang QD, Cox BN. Cohesive models for damage evolution in laminated composites. Int J Fract 2005;133:107–37.
[6] Turon A, Camanho PP, Costa J, Dávila CG. A damage model for the simulation of delamination in advanced composites under variable-mode loading. Mech Mater 2006;38:1072–89.
[7] Jiang W-G, Hallett SR, Green BG, Wisnom MR. A concise interface constitutive law for analysis of delamination and splitting in composite materials and its application to scaled notched tensile specimens. Int J Numer Method Eng 2007;69:1982–95.
[8] van der Meer FP, Sluys LJ. Mesh-independent modeling of both distributed and discrete matrix cracking in interaction with delamination. Engng Fract Mech 2010;77:719–35.
[9] Moës N, Dolbow J, Belytschko T. A finite element method for crack growth without remeshing. Int J Numer Method Eng 1999;46:131–50.
[10] Esna Ashari S, Mohammadi S. Modeling delamination in composite laminates using XFEM by new orthotropic enrichment functions. In: IOP Conference series: materials science and engineering, vol. 10; 2010. p. 012240.
[11] Wells GN, de Borst R, Sluys LJ. A consistent geometrically non-linear approach for delamination. Int J Numer Method Eng 2002;54:1333–55.
[12] Remmers JJC, Wells GN, de Borst R. A solid-like shell element allowing for arbitrary delaminations. Int J Numer Method Eng 2003;58:2013–40.
[13] Chaboche JL, Feyel F, Monerie Y. Interface debonding models: a viscous regularization with a limited rate dependency. Int J Solids Struct 2001;38:3127–60.
[14] Turon A, Dávila CG, Camanho PP, Costa J. An engineering solution for mesh size effects in the simulation of delamination using cohesive zone models. Engng Fract Mech 2007;74:1665–82.
[15] Harper PW, Hallett SR. Cohesive zone length in numerical simulations of composite delamination. Engng Fract Mech 2008;75:4774–92.
[16] van der Meer FP, Sluys LJ, Hallett SR, Wisnom MR. Computational modeling of complex failure mechanisms in laminates, J Compos Mater. doi:10.1177/0021998311410473.
[17] Yang QD, Fang XJ, Shi JX, Lua J. An improved cohesive element for shell delamination analyses. Int J Numer Method Eng 2010;83:611–41.
[18] Crisfield MA, Alfano G. Adaptive hierarchical enrichment for delamination fracture using a decohesive zone model. Int J Numer Method Eng 2002;54:1369–90.
[19] Guiamatsia I, Ankersen JK, Davies GAO, Iannucci L. Decohesion finite element with enriched basis functions for delamination. Compos Sci Technol 2009;69:2616–24.
[20] Samimi M, Dommelen JAWV, Geers MGD. An enriched cohesive zone model for delamination in brittle interfaces. Int J Numer Method Eng 2009;80:609–30.
[21] Willis JR. A comparison of the fracture criteria of Griffith and Barenblatt. J Mech Phys Solids 1967;15:151–62.
[22] Rybicki EF, Kanninen MF. A finite element calculation of stress intensity factors by a modified crack closure integral. Engng Fract Mech 1977;9:931–8.
[23] Irwin GR. Analysis of stresses and strains near the end of a crack transversing a plate. J Appl Mech 1957;24:361–6.
[24] Krueger R. Virtual crack closure technique: history, approach, and applications. Appl Mech Rev 2004;57:109–43.
[25] Shen F, Lee KH, Tay TE. Modeling delamination growth in laminated composites. Compos Sci Technol 2001;61:1239–51.
[26] Xie D, Biggers SB. Strain energy release rate calculation for a moving delamination front of arbitrary shape based on the virtual crack closure technique. Part I: formulation and validation. Engng Fract Mech 2006;73:771–85.
[27] Pietropaoli E, Riccio A. On the robustness of finite element procedures based on virtual crack closure technique and fail release approach for delamination growth phenomena. Definition and assessment of a novel methodology. Compos Sci Technol 2010;70:1288–300.
[28] Zou Z, Reid SR, Soden PD, Li S. Mode separation of energy release rate for delamination in composite laminates using sublaminates. Int J Solids Struct 2001;38:2597–613.
[29] Zou Z, Reid SR, Li S, Soden PD. General expressions for energy-release rates for delamination in composite laminates. Proc Roy Soc London, Ser A 2002;458:645–67.
[30] Zou Z, Reid SR, Li S, Soden PD. Application of a delamination model to laminated composite structures. Compos Struct 2002;56:375–89.
[31] Sethian JA. Level set methods and fast marching methods. second ed. Cambridge University Press; 1999.
[32] Sukumar N, Chopp DL, Moës N, Belytschko T. Modeling holes and inclusions by level sets in the extended finite-element method. Comput Method Appl Mech Eng 2001;190:6183–200.
[33] Moës N, Cloirec M, Cartraud P, Remacle J-F. A computational approach to handle complex microstructure geometries. Comput Method Appl Mech Eng 2003;192:3163–77.

[34] Hansbo A, Hansbo P. A finite element method for the simulation of strong and weak discontinuities in solid mechanics. Comput Method Appl Mech Eng 2004;193:3523–40.
[35] Béchet É, Moës N, Wohlmuth B. A stable Lagrange multiplier space for stiff interface conditions within the extended finite element method. Int J Numer Method Eng 2008;78:931–54.
[36] Mergheim J, Steinmann P. A geometrically nonlinear FE approach for the simulation of strong and weak discontinuities. Comput Method Appl Mech Eng 2006;195:5037–52.
[37] Dolbow J, Harari I. An efficient finite element method for embedded interface problems. Int J Numer Method Eng 2009;78:229–52.
[38] Moonen P, Sluys LJ, Carmeliet J. A continuous-discontinuous approach to simulate fracture processes in quasi-brittle materials. Philos Mag 2008;88:3281–98.
[39] van der Meer FP, Sluys LJ. A phantom node formulation with mixed mode cohesive law for splitting in laminates. Int J Fract 2009;158:107–24.
[40] Ji H, Dolbow JE. On strategies for enforcing interfacial constraints and evaluating jump conditions with the extended finite element method. Int J Numer Method Eng 2004;61:2508–35.
[41] Moës N, Béchet E, Tourbier M. Imposing Dirichlet boundary conditions in the extended finite element method. Int J Numer Method Eng 2006;67:1641–69.
[42] Pradeilles-Duval R-M, Stolz C. Mechanical transformations and discontinuities along a moving surface. J Mech Phy Solids 1995;43:91–121.
[43] Nilsson K-F, Storåkers B. On interface crack growth in composite plates. J Appl Mech 1992;59:530–8.
[44] Ousset Y. Numerical simulation of delamination growth in layered composite plates. Eur J Mech Solids 1999;18:291–312.
[45] Osher S, Fedkiw R. Level set methods and dynamic implicit surfaces. Springer Verlag; 2003.
[46] Broberg KB. Cracks and fracture. San Diego, CA: Academic Press; 1999.
[47] Geuzaine C, Remacle J-F. Gmsh: a three-dimensional finite element mesh generator with built-in pre- and post-processing facilities. Int J Numer Method Eng 2009;79:1309–31.
[48] Guimard J-M, Allix O, Pechnik N, Thévenet P. Characterization and modeling of rate effects in the dynamic propagations of mode-II delamination in composite laminates. Int J Fract 2009;160:55–71.
[49] Verhoosel CV, Remmers JJC, Gutiérrez MA. A dissipation-based arc-length method for robust simulation of brittle and ductile failure. Int J Numer Method Eng 2009;77:1290–321.
[50] Bischoff M, Ramm E. Shear deformable shell elements for large strains and rotations. Int J Numer Method Eng 1997;40:4427–49.
[51] Reeder JR, Crews Jr JR. Mixed-mode bending method for delamination testing. AIAA J 1990;28:1270–6.